Smoothing artificial stress concentrations in voxel-based models of textile composites

Guodong Fang[1], Bassam EI Said[2], Dmitry Ivanov[2], Stephen R. Hallett[2,*]

1) Centre for Composite Materials and Structures, Harbin Institute of Technology, Harbin 150080, China

2) Advanced Composites Centre for Science and Innovation (ACCIS), Department of Aerospace Engineering, University of Bristol, Bristol BS8 1TR, UK

Abstract: Voxel meshing is an effective method to discretise the internal architectures of multi-phase materials. Spurious stresses are however introduced in the vicinity of a multi-material interface due to the stepped, block-like representation of smooth boundaries. A stress averaging technique is presented to eliminate artificial mesh-imposed stress concentrations. The effect of the local averaging domain size, averaging weight function, and mesh dependence is explored. The voxel finite element method with stress averaging is then further developed to study progressive damage propagation and failure analysis of composites. An additional control, based on the failure plane angle of each element, is included to ensure propagation of damage in the direction dictated by the physics of the process rather than mesh artefacts. It is found that the stress averaging technique is an effective way to alleviate local stress concentrations and can ensure correct damage and failure mode prediction when compared to a conformal mesh.

Keywords: A. Fabrics/textiles; B. Stress concentrations; B. Mechanical properties; C. Finite element analysis (FEA); Voxel mesh

1. Introduction

Finite element (FE) analysis is a powerful way to study the mechanical properties of textile composites, such as stiffness, nonlinear progressive damage, strength and fatigue etc. [1-3]. However, if the internal geometry of the composite is too complex, it is difficult to generate a consistent conformal mesh of the interacting composite components. In textile composites, the meso-scale geometry configuration is

* Stephen.Hallett@bristol.ac.uk (Stephen R. Hallett)

complex due to yarns interacting with each other during preforming, draping and consolidation [4]. The resin rich zones between yarns are irregular and highly distorted with extremely high aspect ratios. Usually, a large number of tetrahedral elements are used to discretise such complex geometry, but it is difficult to guarantee the mesh quality, or meshing such shapes can be beyond the capability of state of the art automeshing programs. Therefore, alternative methods have been proposed in the literature to solve the problem of mesh generation for composites with complex meso-scale geometry.

In order to overcome these difficulties, Cox et al. [5, 6] proposed the FE based binary model to study the elastic and nonlinear deformation of 3D interlock woven textile composites. In this model, the yarns were represented by two-node line elements without explicit 3D morphology meshing. Yarn nodes were connected with the effective medium nodes via coupling springs. The advantage of this model is the ability to analyze the behavior of large specimens. Its weakness however is that it cannot obtain the local detailed stress fields for the yarns. Following on from Cox's binary model, other methods have been proposed such as the independent mesh method (IMM) [7] and the domain superposition methods (DST) [8, 9] with direct 3D meshing of the yarns coupled to a matrix material. A common aspect of these methods is that yarns and global volume are meshed independently. However, the connection constraint conditions between the individual yarns and global volume can differ. Methods [7-9] all consider yarns with 3D morphology, meshed explicitly, and can tolerate small errors in the detailed yarn geometry. The weakness of these methods is that they utilize penalty functions to approximate the strain field jump at the interface and these penalty functions may increase the computational burden.

Some novel elements have also been developed to describe the interface strain discontinuity problem in order to circumvent the mesh generation difficulties. One approach, called the Mixed FE Method (MFEM)

[10], also uses regular meshes, in which interfaces between the different constituents are not required to coincide with element boundaries. If an element is cut by an interface, the integration points at the two sides of the interface have different material properties. This numerical strategy can calculate the homogenized parameters and be extended to handle progressive damage analysis. However, due to the different materials at different integration points within one element, the large variation in gradients of local displacement and stress can result in a slow rate of convergence for the MFEM. Another potential strategy originally proposed by Belytschko et al. [11] is the extended finite element method (XFEM), which is based on the concept of partition unity to analyze mesh-independent crack propagation in heterogeneous media with phase boundaries. Belytschko et al. [12] and Moës et al. [13] utilized voxel/pixel based meshing to combine implicit surface descriptions of engineering components in a structured FE analysis. An arbitrary mesh was created, similar to the voxel method. A level set function was then calculated at the nodes of elements to determine the location of the implicit surface. Then enrichment functions were used to modify the structured FE approximations of the displacement field so that a strain field jump at the phase boundary was modeled. However, this method becomes difficult to use for multiple and possibly very complex enrichment schemes necessary for characterizing multiple yarn junctions and sharp corners.

Voxel meshing in contrast to these more advanced numerical formulations is a conceptually straight forward technique to discretise complex geometry of composites, especially for textile reinforcement. A voxel mesh uses a regular grid of elements and the internal yarn architecture is defined by assigning different material properties to the individual elements. Voxel meshes for woven composites with complex geometry can be obtained directly from textile pre-processors such as Texgen [14]. One of the main limitations of this technique is that the mesh size needs to be much smaller than the features of interest,

such as the cross section dimensions of yarns. Voxel meshes can be introduced in IMM, DST, MFEM and XFEM, and also can be directly employed in standard FE to study the effective properties [15, 16] and progressive damage analysis [17, 18] of composites. However, due to the regular grid mesh used, non-orthogonal interfaces will appear stepped, or block-like in nature when the appropriate material properties are assigned to the voxel mesh. When considering the resulting stresses from mechanical loading, spurious stress concentrations will exist in the elements at the interface due to the stepped geometry, resulting in issues with stress continuity. These stress concentrations are highly localized and relatively benign for determining elastic stiffness of textile composites, but have a much higher risk of influencing predictions of failure and progressive damage analysis. Various smoothing algorithms for voxel mesh also have been developed [19, 20]. Charras and Guldberg [21] used the boundary-specific filtering method to improve efficiently local solution accuracy of voxel-based model of complex biological structures, and found that the errors of filtered solutions consistently decreased after mesh refinement. Doitrand et al. [22] recently used a least squares method to interpolate the local non-smoothed voxel element stresses at surrounding integration points. However the interpolation process may remove realistic stress concentrations in elements situated in nearby regions. Thus, it was reported in reference [22] that this smoothing method may influence the predicted damage location. Thus it is necessary to overcome the problem of local stress concentrations if voxel-based meshes model of composites are to be used to analyse their mechanical behavior.

This paper describes a new, simple, direct and robust voxel FE method capable of obtaining accurate stresses at yarn interfaces in a voxel mesh, as well as correct progressive damage and failure analysis, for textile composites. A stress averaging technique is proposed to deal with the spurious stress concentrations

arising. The effect of the local averaging domain size, averaging weight function and mesh dependence of the stress distribution is taken into account. A method for tracking the damage path is further developed to study the progressive damage propagation. A model of a single yarn embedded in a matrix with periodic boundary conditions and a transverse load applied is used as an example to examine the proposed method. The feasibility of the stress averaging technique to deal with composites with more realistic textile architectures is verified using a plain weave composite unit cell model.

2. Meshing issues associated with finite element models of composites

2.1 Artificial stress concentrations in voxel meshes

A representative volume element (RVE) containing a simplified circular cross-section inclusion with yarn properties, embedded in a matrix, is modelled as shown in Fig. 1 to demonstrate the issues that arise in voxel meshes. The longitudinal direction is aligned with the z axiz, and the transverse directions with the x and y axes. The volume fraction of the yarn in the RVE is 60%. The yarn used in this model exhibits transversely isotropic homogeneous symmetry with characteristic effective properties of $E_z = 146.8$GPa, $E_x = 11.4$GPa, $\nu_{zx} = 0.3$, $\nu_{xy} = 0.4$ and $G_{zx} = 6.1$GPa [23]. The properties of the isotropic matrix material surrounding with yarn are $E_m = 3.45$GPa and ν_m =0.35[24]. 8-noded solid elements (Abaqus/Standard element type C3D8R) are used to discretise the RVE and the enhanced hourglass control option is used to prevent spurious zero-energy deformation modes. Periodic boundary conditions are applied in both the longitudinal and transverse directions. Transverse compressive loading is applied in *x* direction.

In order to examine the spurious stresses generated in a voxel FE model, the RVE is discretised by voxel meshing with different mesh densities as shown in Fig. 2(a-c). A conformal mesh FE model was also

created as shown in Fig. 2(d), to be used as a benchmark for verification. Fig. 2 shows the stress distribution in the loading direction for the models with different voxel mesh densities and the conformal mesh model. It can be seen that local stress concentrations appear at the stepped block-like interface between the yarn and matrix. This local stress concentration does not reduce with an increase in voxel mesh density. The minimum values obtained by the voxel mesh are notably lower than that of conformal mesh.

Fig. 3 (a) and (b) show the loading direction stress component for two paths, one along the yarn interface and the other across it. It can be seen that the stresses obtained from voxel meshes with different mesh densities fluctuate and deviate significantly from that of the conformal mesh model. In Fig. 3(b), each hollow symbol corresponds to one node in the voxel mesh model. A step change in the stress exists at the interface. It can be observed, that stresses over a region two voxels wide across yarn interface path for the voxel mesh models deviates from that obtained by the conformal mesh model. Thus, the local stress concentration region in the voxel mesh model is approximately two elements deep at the interface for each different material domain. It should be noted that if the voxel FE model were to be directly used to study progressive damage and failure, the spurious stresses may trigger non-existent damage. In the following sections we show the spurious stresses in the voxel FE models can be eliminated by averaging the local stresses around each element on the material interfaces. This is followed by an examination of the effect of the spurious voxel stresses on the transverse damage in the single yarn model.

A unit cell of plain weave textile composite with complex architectures is also studied. The geometric parameters of the unit cell as shown in Fig. 4(a) are: L=6.27mm, H=0.6864mm. The long and short axial lengths of the elliptical cross-section of yarn are 1.09mm and 0.312mm, respectively. The fiber volume fraction of the unit cell is 0.42 [25]. The FE models with voxel meshes or conformal meshes are generated

by TexGen software. Due to the complexity of the meso-structure of the plain weave textile unit cell, the conformal mesh FE model is discretised by four-node tetrahedral elements. The elastic properties of constituents are: $E_z = 221$GPa, $E_x = 16.6$GPa, $\nu_{zx} = 0.26$, $G_{xy} = 5.89$GPa and $G_{zx} = 8.27$GPa for fiber, $E_m =$ 3.5GPa and ν_m = 0.35 for matrix [25]. The yarn effective properties are obtained by the Chamis formulae with 70% intra-yarn fiber volume fraction. Periodic boundary conditions are applied to the FE model of the unit cell in all three directions and a 0.4% tensile strain is applied in the x direction. A top view of the longitudinal stress field in one yarn (red yarn as seen in Fig. 4(a)) within the unit cell, obtained with different voxel meshes, is shown in Fig. 4(b). The material axis x direction stresses along the yarn surface is also compared along a path, A-A' for the different meshes in Fig. 4(c). There exist severe stress oscillations along the path on the yarn surface and whilst the fine voxel mesh can improve the representation of the yarn shape, the local stress concentrations do not have any improvement. These stress oscillations cause significant deviation from the results obtained by the conformal mesh model.

2.2 Mesh orientation influence on damage propagation direction

2.2.1 Progressive damage model

(1) Damage initiation criterion

The failure mechanisms of yarns can be categorized into longitudinal fiber failure and inter fiber failure, Cuntze and Freund characterized this with their so-called Failure Mode Concept (FMC)[26]. In the present study, only the transverse damage is taken into account due to the RVE only being subjected to an applied transverse load. The transverse matrix failure of the yarn can be predicted, dependent on the magnitude of normal stress σ_n acting on the failure plane, by the bimodal criterion:

$$f_T = \begin{cases} \left(\dfrac{\tau_{nt}}{S_T - \mu_T \sigma_n}\right)^2 + \left(\dfrac{\tau_{n1}}{S_L - \mu_L \sigma_n}\right)^2 \geq 1 & \left(\sigma_n \leq 0\right) \\ \left(\dfrac{\sigma_n}{Y_T}\right)^2 \geq 1 & \left(\sigma_n > 0\right) \end{cases} \tag{1}$$

where, σ_n, τ_{nt} and τ_{n1} are the normal and two shear stresses on the failure plane with angle ϕ_0 as shown in Fig. 5, respectively. μ_L and μ_T are the longitudinal and transverse friction coefficients in the fracture plane, respectively. S_L, S_T and Y_T are the longitudinal shear strength, transverse shear strength and transverse tensile strength, respectively.

The typical values of the fracture plane angle for unidirectional fiber composites under pure compressive loading are in the range of 50°-60° [27]. For simplicity, it is assumed in this paper that the angle ϕ_0 is equal to 53°. The transverse friction coefficient can be related with the fracture plane angle in pure compression, that is $\mu_T = -1/\tan(2\phi_0)$. The longitudinal friction coefficient μ_L can be calculated from the transverse friction coefficient and the longitudinal and transverse shear strengths as proposed by Puck and Schürmann [28], that is $\mu_L = \mu_T S_L / S_T$.

When the yarn is in a complex stress state, the action plane angle ϕ will be a variable. The normal of the action plane is rotating in the x_2x_3 plane as shown in Fig. 5. The values of σ_n, τ_{nt} and τ_{n1} are relevant to ϕ for a given stress state. Thus, Eq. (1) can be rewritten as a function with respect to ϕ.

$$f_T(\phi) = \begin{cases} \left(\dfrac{\tau_{nt}(\phi)}{S_T - \mu_T \sigma_n(\phi)}\right)^2 + \left(\dfrac{\tau_{n1}(\phi)}{S_L - \mu_L \sigma_n(\phi)}\right)^2 \geq 1 & \left(\sigma_n(\phi) \leq 0\right) \\ \left(\dfrac{\sigma_n(\phi)}{Y_T}\right)^2 \geq 1 & \left(\sigma_n(\phi) > 0\right) \end{cases} \tag{2}$$

When ϕ is considered over the interval [-90°, 90°], there must exist a maximum value of $f_T(\phi)$. The fracture angle ϕ_0 is determined by searching for the maximum value of $f_T(\phi)$

$$f_T(\phi_0) = \max f_T(\phi) \quad \text{if } \max f_T(\phi) \geq 1 \tag{3}$$

The extended golden section search method [29] can be adopted to calculate the maximum value of $f_T(\phi)$ over the interval [-90 °, 90 °] in this paper. First, the golden section search is conducted several times to obtain a subinterval $[\phi_1, \phi_3]$. The maximum value of $f_T(\phi)$ is in the subinterval $[\phi_1, \phi_3]$. Then, an arbitrary point ϕ_2 is chosen between ϕ_1 and ϕ_3. And a parabola formula can be generated by the interpolation of the three points ϕ_1, ϕ_2 and ϕ_3. The maximum value of the function $f_T(\phi)$ is close to the maximum value of the parabola formula. Finally, if $f_T(\phi_0) \geq 1$, the fracture angle ϕ_0 can be calculated by

$$\phi_0 \approx \phi_2 - \frac{(\phi_2-\phi_1)^2\left(f_T(\phi_2)-f_T(\phi_3)\right)-(\phi_2-\phi_3)^2\left(f_T(\phi_2)-f_T(\phi_1)\right)}{2\left((\phi_2-\phi_1)\left(f_T(\phi_2)-f_T(\phi_3)\right)-(\phi_2-\phi_3)\left(f_T(\phi_2)-f_T(\phi_1)\right)\right)} \tag{4}$$

For the matrix material only, the maximum and minimum principle stress criteria are adopted as a damage initiation criterion, which can be expressed as

$$f_{Mt} = \frac{\sigma_1}{M_1} \geq 1, \qquad f_{Mc} = \frac{|\sigma_3|}{M_3} \geq 1 \tag{5}$$

where σ_1 and M_1 are the maximum principle stress and strength of matrix, respectively. σ_3 and M_3 are the minimum principle stress and strength of matrix, respectively.

(2) Constitutive tensor of damaged material and damage evolution model

In order to characterize the different damage modes, Murakami's damage tensor, which has previously been used to describe damage in textile composites [30], is adopted and can be expressed as

$$\mathbf{D} = \sum_i D_i \mathbf{n}_i \otimes \mathbf{n}_i \quad (\mathrm{i} = 1,2,3) \tag{6}$$

where, D_i and $\mathbf{n}_i$ are the principal value and principal unit vector of the damage tensor. The symmetric effective stress can be written as

$$\bar{\boldsymbol{\sigma}} = \left[(\mathbf{I} - \mathbf{D})^{-1} \cdot \boldsymbol{\sigma} + \boldsymbol{\sigma} \cdot (\mathbf{I} - \mathbf{D})^{-1} \right] / 2 \tag{7}$$

The Eq. (7) also can be rewritten as

$$\bar{\boldsymbol{\sigma}} = \mathbf{M}(D) : \boldsymbol{\sigma} \tag{8}$$

Based on the equivalent elastic complementary energy theory, the compliance matrix of the damaged material can be derived as

$$\mathbf{S}(D) = \mathbf{M}^{\mathrm{T}}(D)\, \mathbf{S}\, \mathbf{M}(D) \tag{9}$$

Then, inverting the compliance matrix, the stiffness matrix of the damaged material $C(D)$ can be expressed in matrix form by using the components of the stiffness matrix of undamaged material and the principal value of the damage tensor D_i [31], which can be explicitly represented as

$$C(D) = \begin{bmatrix} b_1^2 Q_{11} & b_1 b_2 Q_{12} & b_1 b_3 Q_{13} & 0 & 0 & 0 \\ & b_2^2 Q_{22} & b_2 b_3 Q_{23} & 0 & 0 & 0 \\ & & b_3^2 Q_{33} & 0 & 0 & 0 \\ & sym & & b_{12} Q_{44} & 0 & 0 \\ & & & & b_{31} Q_{55} & 0 \\ & & & & & b_{23} Q_{66} \end{bmatrix} \tag{10}$$

where, D_i $(i = 1,2,3)$ is the damage variable in the local material coordinate system. $b_1 = 1 - D_1$, $b_2 = 1 - D_2$, $b_3 = 1 - D_3$, $b_{12} = \left(\frac{2(1-D_1)(1-D_2)}{2 - D_1 - D_2} \right)^2$, $b_{23} = \left(\frac{2(1-D_2)(1-D_3)}{2 - D_2 - D_3} \right)^2$, $b_{31} = \left(\frac{2(1-D_3)(1-D_1)}{2 - D_3 - D_1} \right)^2$, $Q_{ij}, (i, j = 1,2,3)$ is the component of stiffness matrix of undamaged material.

When the damage propagation analysis is implemented by using FE implicit algorithm, the rapid change of damage variables may induce numerical convergence problems. An effective method to improve numerical convergence is an artificial viscous model [32], which can be used to delay the damage

development by introducing a viscous coefficient. The time derivatives of the damage variables D_i $(i=1,2,3)$ can be written as

$$\dot{D}_i = \frac{1}{\eta_i}(\Omega_i - D_i) \qquad i=(1,2,3) \tag{11}$$

where, η_i is the viscosity coefficient recognized as the relaxation time of the viscous model, D_i and Ω_i are the regularized damage variable and realistic damage variable for damage mode i, respectively. The regularized damage variables are used in stiffness matrix of the damaged material. If the viscosity parameter is a small value compared to the time increment, the numerical convergence of the model will have a significant improvement without sacrificing numerical accuracy greatly. In this paper, the viscosity coefficient is set equal to 0.0001s.

In the present study, $\Omega_1=\Omega_2=\Omega_3=d_M$, d_M is the matrix damage initiated by the criterion in Eq. (5). For the yarn, we do not consider the longitudinal direction damage, so $D_1=0.0$. When the single yarn model has an applied transverse loading, transverse damage, d_T, of the yarn can be initiated by the criterion in Eq. (1). The damage variables in the local material coordinate system, Ω_i, of the yarn can be written as

$$\Omega_2=\Omega_3=d_T \tag{12}$$

The evolution law for the damage variable $d_s\ (s=T,M)$ [33] can be written as

$$d_s = 1-\frac{\delta_s^0}{\delta_s}\left[1-\left(1-\exp\left(\frac{\delta_s-\delta_s^0}{\delta_s^f-\delta_s^0}\right)\right)\Big/\left(1-\exp(1)\right)\right] \tag{13}$$

where, δ_s is the equivalent displacement, δ_s^0 and δ_s^f are the displacements corresponding to initial damage and final failure, respectively.

Using the crack band theory of Bazant et al [34], the element dissipated energy is set equal to the

material fracture energy when the element has failed, which can be written as

$$\frac{1}{2}\bar{\varepsilon}_s^f \bar{\sigma}_s^f l^3 = G_C^s l^2 \tag{14}$$

where, l is the characteristic length of element, which is the cube root of element volume for cubic voxel elements, G_C^s is the fracture energy, $\bar{\sigma}_s^f$ and $\bar{\varepsilon}_s^f$ are the equivalent peak stress and maximum equivalent strain, respectively.

The equivalent displacement will thus vary with element size, and is defined as

$$\delta_s = \bar{\varepsilon}_s l \tag{15}$$

The initial equivalent displacement is the value of Eq. (15) when the damage initiation criterion equals to one, that is $\delta_s^0 = \delta_s\big|_{f_s=1}$. Using the Eq. (14) and Eq. (15), the maximum equivalent displacement at failure can be written as $\delta_s^f = \bar{\varepsilon}_s^f l = 2G_C^s / \bar{\sigma}_s^f$. The equivalent strain and equivalent peak stress [35,36] can be expressed as

$$\begin{cases} \bar{\varepsilon}_T = \sqrt{\varepsilon_n^2 + \gamma_{n1}^2 + \gamma_{nt}^2} \quad \text{and} \quad \bar{\sigma}_T^f = \sqrt{\sigma_n^2 + \tau_{n1}^2 + \tau_{nt}^2}\Big|_{f_T=1} \quad (\sigma_n \le 0) \\ \bar{\varepsilon}_T = \varepsilon_n \quad \text{and} \quad \bar{\sigma}_T^f = \sigma_n\big|_{f_T=1} \quad (\sigma_n > 0) \\ \bar{\varepsilon}_M = \varepsilon_1 \quad \text{and} \quad \bar{\sigma}_M^f = \sigma_1\big|_{f_{Mt}=1} \\ \bar{\varepsilon}_M = -\varepsilon_3 \quad \text{and} \quad \bar{\sigma}_M^f = -\sigma_3\big|_{f_{Mc}=1} \end{cases} \tag{16}$$

2.2.2 Damage development path of the RVE with different conformal meshes

Based on the damage model in the Section 2.2.1, the progressive damage and failure analysis of the RVE under a transverse compressive load has been carried out. The strength parameters of the constituents within the RVE model in Section 2.2.1 are Y_T =66.5MPa, $S_T = S_L$ =58.7MPa, M_1 =80MPa, M_3 =240MPa, G_C^{T-} =0.76N/mm and G_C^{T+} =0.23N/mm [23]. After damage is initiated at an element in the RVE, damage will propagate into neighboring elements with an increase in applied load. The

damage development path is thus gradually formed during the analysis. The damage development path may however depend on the orientation of the mesh used. Fig. 6 provides the predicted damage development path of RVE with different conformal mesh models under compressive loading in the x direction. Four different conformal meshes for the RVE were considered in this analysis, with the central region's element mesh orientation being 0°, 15°, 30° and 45° with respect to the x direction. The material axis orientation for the yarn remains unchanged in the each conformal mesh model. It can be seen from Fig. 6 that the damage development path is significantly influenced by the local mesh direction in the RVE model. Based on the Puck criterion, the failure plane angle should be approximately 50°. When the centre elements are nearly parallel to the failure plane angle, the damage development path is only one element wide, such as the 45° mesh.

3. Local stress averaging technique

3.1 Method and implementation

In the absence of a local discontinuity such as damage, crack, sharp geometric change or material boundary a model with a consistent material should have a smoothly varying local stress. A change in material will cause a sharp change in stress, but for a model discretised by a voxel mesh it can be seen that stresses around such an interface thus become further disrupted as shown in Fig. 3(a), resulting in local stress concentrations. This is caused by the element boundaries forming an irregular non-smooth surface. Here we propose to employ stress averaging technique to alleviate these spurious local stresses. This is a reasonable approach since overall the system remains in equilibrium and the averaging impact is limited to the local vicinity of the stress concentration. For the elements close to such an irregular interface, a stress averaging scheme can be conducted over a local domain around each element to approximate the realistic

stress, which can be expressed as

$$\bar{\sigma} = \frac{\int_{\Omega} f(\sigma_{ij}) \varphi(\vec{r}) \, dV}{\int_{\Omega} \varphi(\vec{r}) \, dV} \tag{17}$$

where, $f(\sigma_{ij})$ is the stress function, $\varphi(\vec{r})$ is the weight function, Ω is the local averaging domain, $\vec{r}$ is a vector pointing from the centre the element of interest to other elements in the local domain.

It should be noted that the elements in the local domain should be of the same material, as shown in Fig. 7(a), because only these elements can be considered to have a continuously changing stress level. From the plot in Fig. 3(b) it can be seen that for the voxel mesh the stress distribution in elements further from the material interface are sufficiently accurate. Therefore, only two layers of elements adjacent to the material interface should be considered for this stress averaging treatment as shown in Fig. 7(b). It is necessary to determine the size of the averaging domain and the weight function for the stress averaging technique. In this paper, we adopt and examine three kinds of weight function forms: linear $\varphi(\vec{r}) = 1 - |\vec{r}| / |\vec{r}|_{\max}$, exponent $\varphi(\vec{r}) = \exp(-|\vec{r}| / |\vec{r}|_{\max})$ and constant $\varphi(\vec{r}) = 1$. For the different density voxel meshes, it is difficult to determine directly a constant size for the local averaging domain. It is however possible to use the element layers around a given element. Therefore, one layer, two layers and three layers of elements surrounding an element of interest, as shown in Fig. 8, are recognized as three different sizes of averaging domain to be considered. The local averaging domain sizes thus depend on the mesh size.

The stress averaging does not change the finite element computation based on the voxel meshes, but can be considered as a post-processing treatment on the spurious stresses at the end of each increment. The averaged stress of an element can then be used to identify whether it is damaged or not. It should be noted

that if the element is damaged it is excluded from the stress averaging algorithm and its adjacent elements will also not use the stresses of the damaged element in averaging. In the present study, the stress averaging treatment is implemented in the commercial FE software ABAQUS/Standard. The computation process is as follows: Firstly, element information, such as element number, element centre coordinates, and each element volume in the local averaging domain, should be gathered. Then, the element information is read into the ABAQUS global variables by using the Fortran common block in the ABAQUS UEXTERNALDB subroutine at the start of computation, which can be accessed by element in the voxel model. Finally, the stress averaging can be conducted at each element integration point by using ABAQUS USDFLD or UMAT subroutines. It should be noted that the stress averaging technique does not increase the nodal degrees of freedom or the number of integration points during the computation. It only increases the computation for gathering element information before computation and for the stress averaging at each increment during the calculation.

3.2 Stress analysis of voxel FE model with stress averaging

After a 0.5% compressive strain is applied to the RVE in the x direction, the distribution of averaged stress in the x compressive loading direction of RVE with different voxel meshes can be obtained as shown in Fig. 9. Here two layers of elements around each element of interest are averaged using an exponent weight function. Comparing with the stress distributions against those in Fig. 2, it can be seen that the averaging stress distributions give a significant improvement. The local stress concentration close to the material interface is nearly eliminated. The maximum and minimum stress obtained by the three voxel meshes and conformal mesh models are as given in Tab. 1, in which the two element layer averaging domain and exponent weight function are adopted. Although the averaged stress distributions for the different voxel

meshes are slightly different from the results obtained from the conformal mesh, the maximum and minimum averaged stress values are acceptable to use in a progressive damage analysis.

Fig. 10 shows the effect of different averaging domain sizes on the average stress along path 1 of the RVE, using the coarse voxel FE mesh. The exponent form of the averaging weight function was used. It can be seen that the stress components at the interfacial elements along path 1 all have a good improvement after the stress averaging technique. The averaging domain sizes has some influence on the stress averaging results, with generally the larger averaging domain giving a result closer to the conformal mesh model. The normal S_{yy} stress and shear S_{xy} stress along path 1 after stress averaging treatment have the greatest deviation from the conformal mesh, but their absolute values are relatively small since these are introduced by Poisson's contraction only.

The two-layer averaging was chosen as the most suitable to take forward since this gives sufficiently accurate results, but with a reduced computational cost compared to the three-layer averaging. This technique was then use to study the influence of mesh size, since for failure analysis it is important to have a mesh objective formulation. Fig. 11 shows the result of stress averaging in the x loading direction for different voxel mesh densities. The exponent form of the averaging weight function was also used here. It can be seen that although the absolute size of the stress averaging domain varies with the mesh size, overall it produces good results for all mesh densities. As perhaps can be expected, the best results are obtained with the finest mesh, but the coarse and medium mesh results are also acceptable. The effect of the averaging weight function used for the stress averaging scheme is also considered and shown in Fig. 12. After calculation, the effect of varying the averaging weight function is small, but from the stress contribution view, the linear and exponent forms are more reasonable. Above all, it can be seen that the

stress averaging does indeed give useful results. Now, a reasonable stress field has been achieved to apply a progressive damage model in the following section.

For the unit cell model of a plain weave textile composite, the stress fields of a yarn (red yarn in Fig. 4(a)) are provided in Fig. 13(a). Different voxel and conformal mesh sizes are taken into account. It should be noted that some distorted tetrahedral elements exist in the conformal mesh model. And these elements also can induce stress concentrations. The predictions of the conformal mesh model have some dependence on mesh size and the coarse mesh cannot guarantee the accurate results. The two-layer exponential form of the averaging weight function is adopted for the voxel-based model. The stress field distributions of voxel-based model after stress averaging are similar to the conformal mesh model. The maximum stress of the voxel based model after stress averaging is however slightly lower than that obtained by conformal mesh model, but unlike the case of artificial voxel stress concentrations these stress values improve towards the conformal mesh values with mesh refinement. Fig. 13(b) provides the stresses along a path on the yarn surface. The path stresses of the voxel-based model after stress averaging have greatly alleviated the serve oscillations as shown in Fig. 4(c), and they are close to the path stresses obtained by conformal mesh model. Fig. 14 shows cross-section stress contours of the models with different meshes. It can be seen that the stress concentrations are obvious at the boundaries between yarn and matrix for voxel-based model with coarse and fine meshes. After stress averaging treatment, the stress contours are similar to the conformal mesh models. This shows that the stress averaging treatment can effectively alleviate the spurious stresses at the boundaries due to the voxel meshes for more realistic and complex textile geometries.

4. Tracking damage development path

Damage usually initiates at the first point that satisfies the above damage initiation criterion. The

damage should then propagate at the failure plane angle of that point. Damage cannot however be introduced suddenly as this can lead to convergence problems in ABAQUS/Standard. Thus, viscous regularization, as given in Eq. (11), is usually introduced to delay the damage development. This may however have the unintended consequence that the elements surrounding the initially damaged element will satisfy the initiation damage criterion as well, due to the delay in energy dissipation. For transverse damage of the yarn the local mesh orientation also has an effect on the direction of crack propagation, with cracks tending to follow the mesh lines rather the predicted fracture angle as mentioned in Section 2.2.2. An algorithm is thus introduced to prevent this. When an element is damaged, a local domain two layers of elements deep surrounding that element is defined. Within this zone only those elements in line with the fracture angle, ϕ_0, may further initiate damage (as shown in Fig.15), thus alleviating the mesh orientation bias. Beyond the local domains defined around damaged elements, damage can freely initiate and new damage centres, with new local domains can be further established. It should be noted that the new local domain may include elements which are members of already existing local domain associated with other elements. The elements in the new local domain are tagged, again based on the failure plane angle of the new damage centre element as shown in Fig.15. Looping over this procedure, the damage path can be obtained, and multiple damage paths can be allowed to join together.

Fig. 16 is the computation flow chart for the progressive damage and failure analysis by using a voxel FE model with the stress averaging technique and damage path tracking method, which can be divided into three main parts. Firstly, the preprocessor part is used to gather the element information for averaging the stresses and tracking the damage path. In the second part, based on the damage initiation criterion, the integration point of an element is identified as whether it has been damaged or not. The damage variables

of the element integration point are then updated by the damage evolution law. The third part concerns tagging the damage path elements in a local damage domain surrounding each damaged element at the end of each increment. In the computation, the element stresses and strains are obtained by the Newton-Raphson incremental method and the damage variables are introduced through an ABAQUS UMAT subroutine. After the convergence criterion is reached by several equilibrium iterations, the analysis goes to the next increment.

Fig. 17 is the predicted damage development path of RVE with different conformal mesh models under compressive loading in the x direction. The damage path tracking method is implemented to compare with damage being allowed to development freely. After the damage tracking scheme is adopted, the mesh dependence of the damage path is improved. Although the damage path is still quite wide for certain meshes, the direction of damage development is improved. It can thus be seen that where very regular meshes are used, as in the case of voxel analyses, such crack path tracking algorithms can improve results.

5. Comparing the damage analysis of the RVE with voxel and conformal meshes

The following cases have been considered for progressive damage analysis of the RVE: the conformal mesh model, using a voxel mesh directly and using a voxel mesh combined with stress averaging. The results obtained from the conformal mesh are used as a verification baseline for the other cases. The stress averaging treatment for voxel meshes here uses an exponent weight function and a two element deep local averaging domain. In addition, the effect of voxel mesh density and loading conditions on the progressive damage analysis of the RVE is studied. The damage path tracking method is implemented to deal with the multiple damage path junctions, and ensure a mesh independent damage development direction.

Fig. 18(a) and Fig.19(a) show the normalized macroscopic stress vs normalized strain curve of the

RVE with different meshes under transverse compressive stress and combined compressive and shear stress, respectively, in which σ_0 and ε_0 correspond to the maximum stress and strain at the maximum stress of the results obtained from the conformal mesh. It can be seen that the slope of the curves do not have any notable differences for the different meshes. It can thus be concluded that the voxel FE model can be used directly to predict the effective elastic properties of composites. When only transverse compressive loading is applied to the RVE with different meshes, almost the same peak values are obtained by all of the voxel meshes, as shown in Fig. 18(a). The peak value of the fine voxel mesh is closest to that obtained by smooth interface FE model as shown in the magnified view of Fig. 18(a). The stress and strain response obtained from the voxel mesh with stress averaging is same as without stress averaging for each voxel mesh density. Fig. 18(b) shows the damage development path for the different meshes under only compressive loading. In this case, the damage development paths in the RVE appear to be independent from the voxel mesh density, stress averaging treatment and conformal meshing. In this case the spurious stresses of the voxel mesh do not influence the failure of the RVE since damage initiates in the centre of the yarn, away from the multi-material interface.

Fig. 19(a) shows the normalized stress values from the RVE under combined compressive and shear displacement for different voxel meshes and the conformal mesh. The applied macroscopic compressive strain is equal to the macroscopic shear strain. In the results obtained directly from the voxel mesh without stress averaging the yarn fails at a slightly lower load. After stress averaging treatment, the peak value for each voxel model is closer to that of the conformal mesh model. With an increase in voxel mesh density, the stress-strain response obtained by the voxel models with stress averaging has little increase as well. In contrast to the small differences in failure load between models, an examination of the damage and failure

modes in Fig. 19(b) shows significant differences. In the RVE using the voxel mesh without stress averaging treatment damage is initiated at the material interface in elements with spurious stress oscillations. In contrast, after stress averaging treatment, the initiation location of damage in the voxel meshes is same as that from the conformal mesh. The damage development path also follows a similar pattern although there are some small differences for damage distribution with different voxel mesh densities.

From these results it can be concluded that the stress averaging treatment for voxel models gives improved results for the prediction of progressive damage when failure initiates from the location of spurious stress oscillation caused by the voxelisation. This is dependent on the loading conditions applied but for the general case and robust analysis it overall gives an improved result, with no detriment to cases where failure does not initiate from these locations.

6. Conclusions

The stress averaging technique is an effective, simple and direct method to correct the spurious stresses introduced by the stepped block-liked interface at material junctions in voxel finite element models, which does not increase the number of integration points. This stress averaging technique is also shown to be relatively mesh independent. If the local averaging domain is too large, the maximum averaged stress will lower the accuracy of results. If the averaging domain is too small, the local stress concentration still exists. It is found in the present study that a depth of two elements surrounding the element of interest is the best choice for the local averaging domain. From the stress contribution view, the linear and exponent forms are suitable to use as average weight functions. These spurious stresses can significantly change the damage and failure modes. The initial damage location and development path for such voxel models has been verified against results obtained from a conformal mesh model of the same geometry. The results shown by

voxel meshing combining stress averaging and damage tracking algorithm are as good as those obtained with conventional meshing techniques. Interfacial failure between the yarn and the matrix was not treated separately to the yarn and matrix damage models in the analyses presented here. This would require the insertion of specialist cohesive interface elements, which is not feasible with the block-like interfaces created in the voxel meshing technique. Yarn disbond can however still occur, through failure of the boundary layer of elements in the yarn or matrix, as a special case of the failure criteria in equations 2 and 5. Figure 13 shows that the stress averaging technique captures the stress state at the yarn interface well, required for this mode of failure. If there was a genuine stress concentration at the interface causing failure, then it would have to be highly localized (less than 2 layers of elements wide) before the stress averaging technique would artificially smooth it over and delay initiation of damage. In such cases the exponential weighting function may be more appropriate, to take account of the high local stress gradient. Stress discontinuities due to a change of material are still captured, since the averaging is only performed over elements with the same material type.

Compared to the use of a conformal mesh, voxel models are thus much more general for composites with very complex internal geometry that needs to be included in the mesh. This technique can thus be further developed to study progressive damage in textile composites with weave architectures more complex than the simple unit cell presented here for verification.

Acknowledgement

Support for this work by the State Scholarship Fund from the China Scholarship Council (CSC), National Natural Science Foundation of China (11102051) is gratefully acknowledged.

References

[1] Tan P, Tong L, Steven GP. Modelling for predicting the mechanical properties of textile composites—A review. Composites Part A: Applied Science and Manufacturing. 1997;28(11):903-22.
[2] Onal L, Adanur S. Modeling of Elastic, Thermal, and Strength/Failure Analysis of Two-Dimensional Woven Composites—A Review. Applied Mechanics Reviews. 2007;60(1):37-49.
[3] Fang G, Liang J. A review of numerical modeling of three-dimensional braided textile composites. Journal of Composite Materials. 2011:0021998311401093.
[4] El Said B, Green S, Hallett SR. Kinematic modelling of 3D woven fabric deformation for structural scale features. Composites Part A: Applied Science and Manufacturing. 2014;57(0):95-107.
[5] Xu J, Cox BN, McGlockton MA, Carter WC. A binary model of textile composites—II. The elastic regime. Acta Metallurgica et Materialia. 1995;43(9):3511-24.
[6] McGlockton MA, Cox BN, McMeeking RM. A Binary Model of textile composites: III high failure strain and work of fracture in 3D weaves. Journal of the Mechanics and Physics of Solids. 2003;51(8):1573-600.
[7] Iarve EV, Mollenhauer DH, Zhou EG, Breitzman T, Whitney TJ. Independent mesh method-based prediction of local and volume average fields in textile composites. Composites Part A: Applied Science and Manufacturing. 2009;40(12):1880-90.
[8] Nakai H, Kurashiki T, Zako M. Individual modeling of composite materials with mesh superposition method under periodic boundary condition. Proceedings of the 16th International Conference on Composite Materials (ICCM-16), 2007.
[9] Jiang WG, Hallett S, Wisnom M. Development of Domain Superposition Technique for the Modelling of Woven Fabric Composites. Mechanical Response of Composites: Springer Netherlands; 2008. p. 281-91.
[10] Lippmann N, Steinkopff T, Schmauder S, Gumbsch P. 3D-finite-element-modelling of microstructures with the method of multiphase elements. Computational Materials Science. 1997;9(1–2):28-35.
[11] Belytschko T, Black T. Elastic crack growth in finite elements with minimal remeshing. International Journal for Numerical Methods in Engineering. 1999;45(5):601-20.
[12] Belytschko T, Parimi C, Moës N, Sukumar N, Usui S. Structured extended finite element methods for solids defined by implicit surfaces. International Journal for Numerical Methods in Engineering. 2003;56(4):609-35.
[13] Moës N, Cloirec M, Cartraud P, Remacle JF. A computational approach to handle complex microstructure geometries. Computer Methods in Applied Mechanics and Engineering. 2003;192(28–30):3163-77.
[14] Lin H, Zeng X, Sherburn M, Long AC, Clifford M. Automated Geometric Modelling of Textile Structures. Textile Research Journal. 2012;82(16):1689-702.
[15] Gao X, Luo P, Yu G, Fang G, Song Y. Micro-XCT-based finite element method for prediction of elastic modulus of plane woven carbon fiber-reinforced ceramic matrix composites. Journal of Composite Materials. 2014: 0021998314562631.
[16] De Carvalho NV, Pinho ST, Robinson P. Reducing the domain in the mechanical analysis of periodic structures, with application to woven composites. Composites Science and Technology. 2011;71(7):969-79.
[17] Green SD, Matveev MY, Long AC, Ivanov D, Hallett SR. Mechanical modelling of 3D woven composites considering realistic unit cell geometry. Composite Structures. 2014;118:284-93.
[18] Koumpias AS, Tserpes KI, Pantelakis S. Progressive damage modelling of 3D fully interlaced woven composite materials. Fatigue & Fracture of Engineering Materials & Structures. 2014;37(7):696-706.

[19] Camacho DL, Hopper RH, Lin GM, Myers BS. An improved method for finite element mesh generation of geometrically complex structures with application to the skullbase. Journal of biomechanics. 1997;30(10):1067-70.
[20] Boyd SK, Muller R. Smooth surface meshing for automated finite element model generation from 3D image data. Journal of biomechanics. 2006;39(7):1287-95.
[21]Charras GT, Guldberg RE. Improving the local solution accuracy of large-scale digital image-based finite element analyses. Journal of biomechanics. 2000;33(2):255-9.
[22] Doitrand A, Fagiano C, Irisarri FX, Hirsekorn M. Comparison between voxel and consistent meso-scale models of woven composites. Composites Part A: Applied Science and Manufacturing. 2015;73:143-54
[23] Maimí P, Camanho PP, Mayugo J, Dávila C. A continuum damage model for composite laminates: Part II–Computational implementation and validation. Mechanics of Materials. 2007;39(10):909-19.
[24] Fang GD, Liang J, Lu Q, Wang BL, Wang Y. Investigation on the compressive properties of the three dimensional four-directional braided composites. Composite Structures. 2011;93(2):392-405.
[25]Ito M, Chou T-W. An Analytical and Experimental Study of Strength and Failure Behavior of Plain Weave Composites. Journal of Composite Materials. 1998;32(1):2-30.
[26] Cuntze R, Freund A. The predictive capability of failure mode concept-based strength criteria for multidirectional laminates. Composites Science and Technology. 2004;64(3):343-77.
[27] González C, Llorca J. Mechanical behavior of unidirectional fiber-reinforced polymers under transverse compression: Microscopic mechanisms and modeling. Composites Science and Technology. 2007;67(13):2795-806.
[28] Puck A, Schürmann H. Failure analysis of FRP laminates by means of physically based phenomenological models. Composites Science and Technology. 2002;62(12–13):1633-62.
[29] Wiegand J, Petrinic N, Elliott B. An algorithm for determination of the fracture angle for the three-dimensional Puck matrix failure criterion for UD composites. Composites Science and Technology. 2008;68(12):2511-7.
[30]Ivanov DS, Lomov SV. Modelling the structure and behaviour of 2D and 3D woven composites used in aerospace applications, in Polymer Composites in the Aerospace Industry, P.E. Irving and C. Soutis, Editors. 2015, Elsevier - Woodhead Publishers: Cambridge. p. 21-52.
[31] Zako M, Uetsuji Y, Kurashiki T. Finite element analysis of damaged woven fabric composite materials. Composites Science and Technology. 2003;63(3):507-16.
[32] Duvaut G. Inequalities in mechanics and physics / G. Duvaut, J. L. Lions ; translated from the French by C. W. John. Berlin ; New York: Springer-Verlag; 1976.
[33] Abaqus User Manual Version 6.14. USA.: Dassault Systemes Simulia Corp., 2014
[34] Bažant Z, Oh BH. Crack band theory for fracture of concrete. Matériaux et Construction. 1983;16(3):155-77.
[35] Lapczyk I, Hurtado JA. Progressive damage modeling in fiber-reinforced materials. Composites Part A: Applied Science and Manufacturing. 2007;38(11):2333-41.
[36] Fang GD, Liang J, Lu Q, Wang BL, Wang Y. Investigation on the compressive properties of the three dimensional four-directional braided composites. Composite Structures. 2011;93(2):392-405.

Figures:

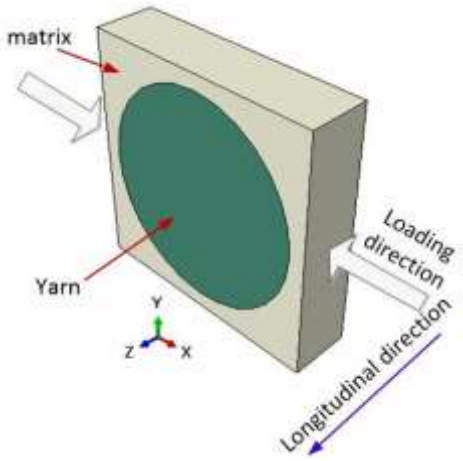

Fig. 1 Geometry of a single yarn embedded in matrix

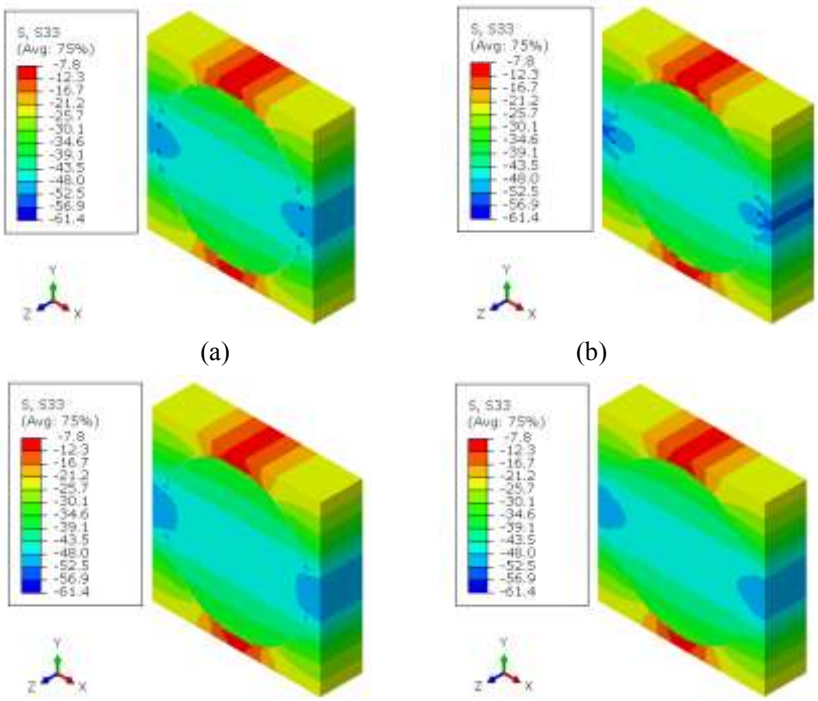

Fig. 2 Stress distribution of x direction stress component, (a) coarse voxel mesh, (b) medium voxel mesh, (c) fine voxel mesh, (d) conformal mesh

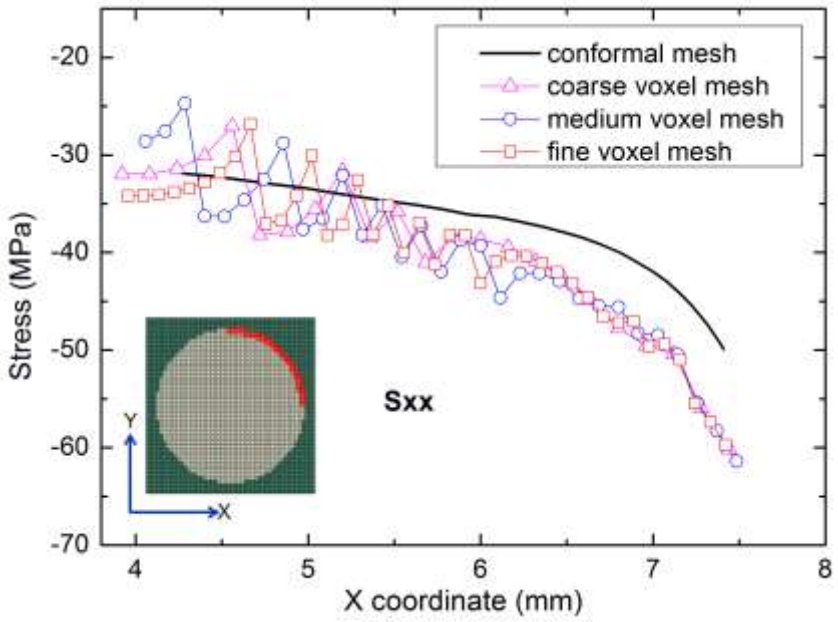

(a)

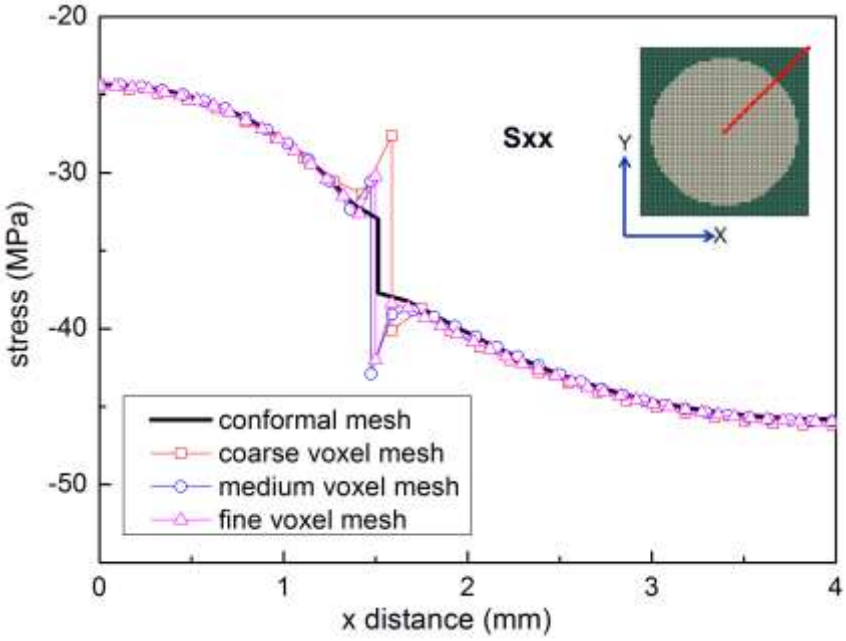

(b)

Fig. 3 Path stress (x loading direction stress component), (a) path 1, (b) path2.

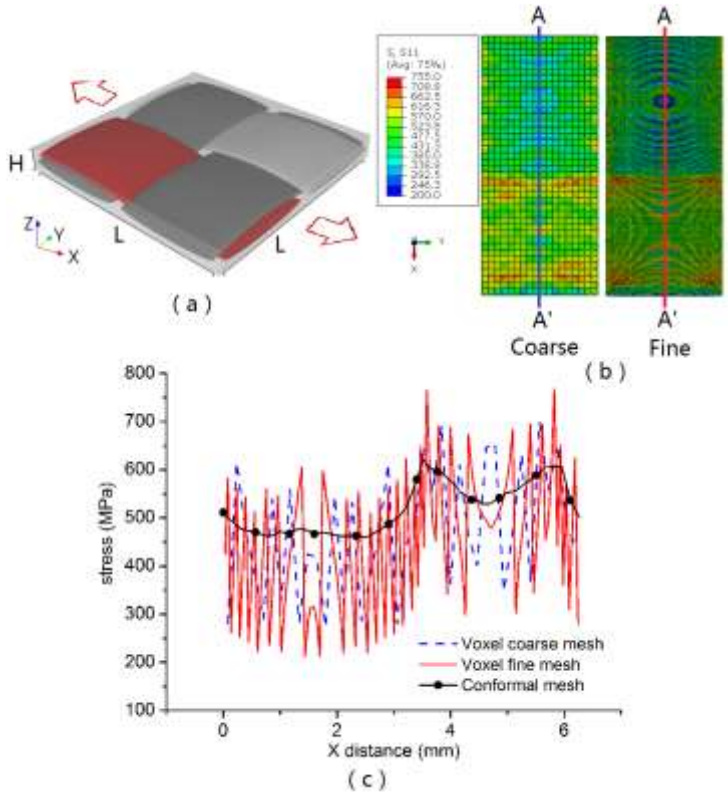

Fig. 4 Plain weave textile composite model, (a) unit cell, (b) *Sxx* stress contours for coarse and fine voxel meshes, (c) *Sxx* stress along the yarn surface path A-A'

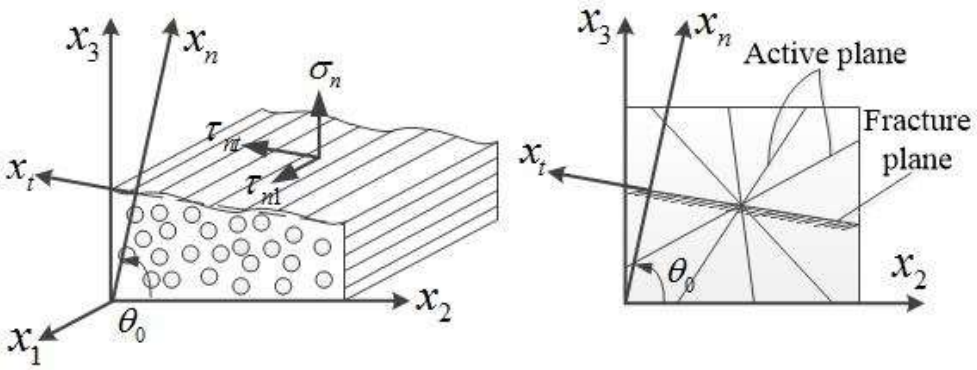

Fig. 5 Action planes and fracture plane angle

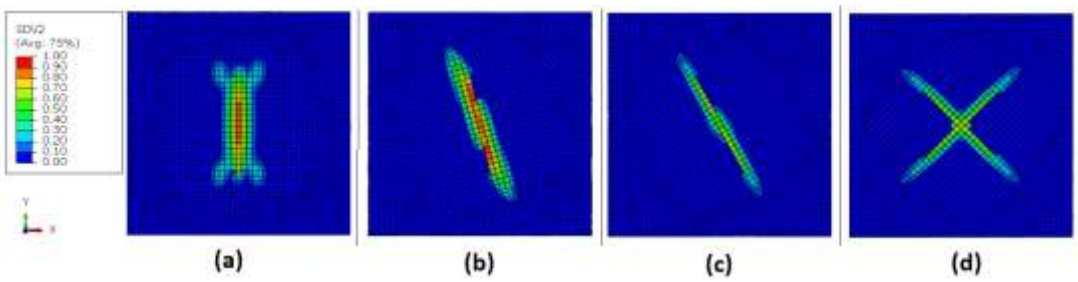

Fig. 6 The mesh Damage development path of RVE with different conformal mesh, (a)0°, (b) 15°,(c) 30°,(d)45°.

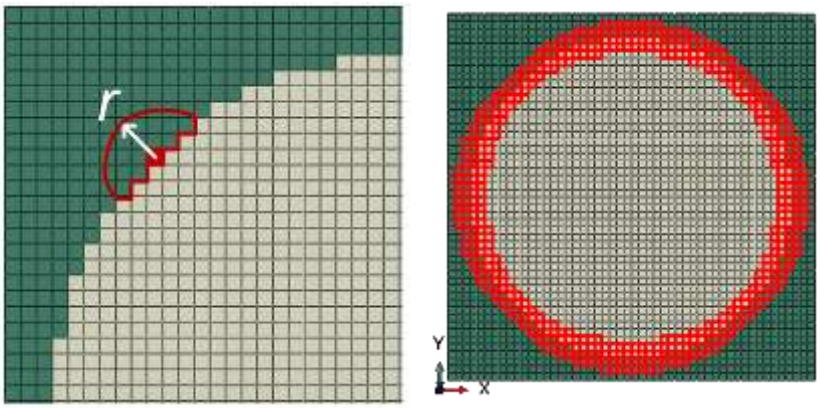

(a) (b)

Fig. 7 Local averaging domain for elements with spurious stress, (a) local averaging domain, (b) elements with spurious stress

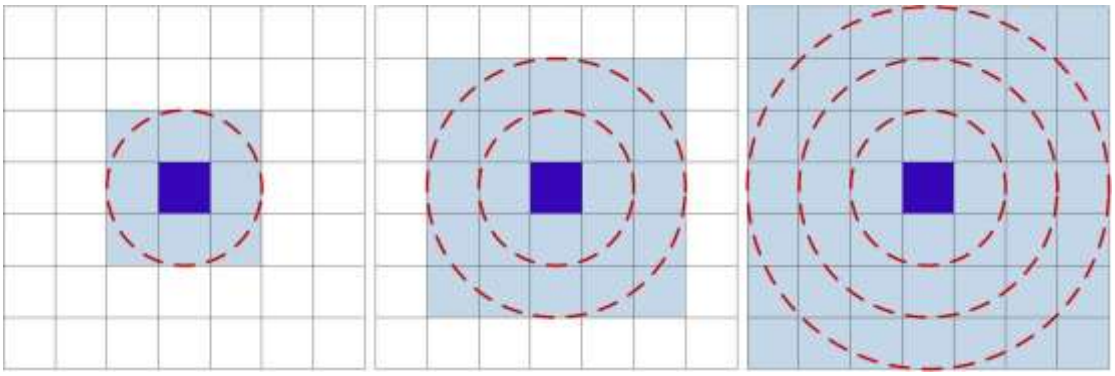

(a) (b) (c)

Fig. 8 Local averaging domain, (a) one layer, (b) two layers, (c) three layers

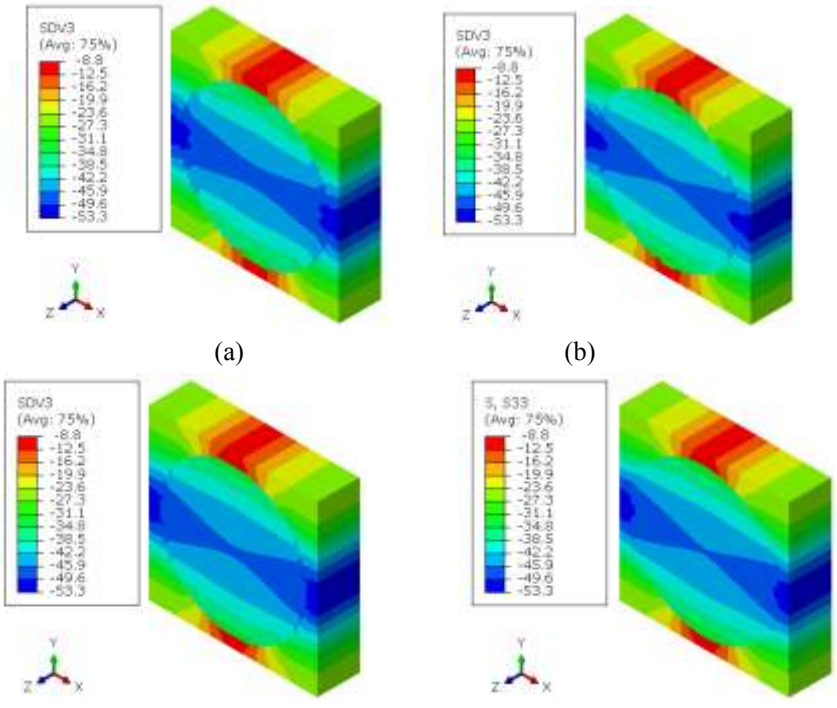

(a) (b)

(c) (d)

Fig. 9 Averaged stress distribution of RVE with different voxel meshes, (a) coarse mesh, (b) medium mesh, (c) fine mesh (d) add in conformal mesh here too for easier comparison

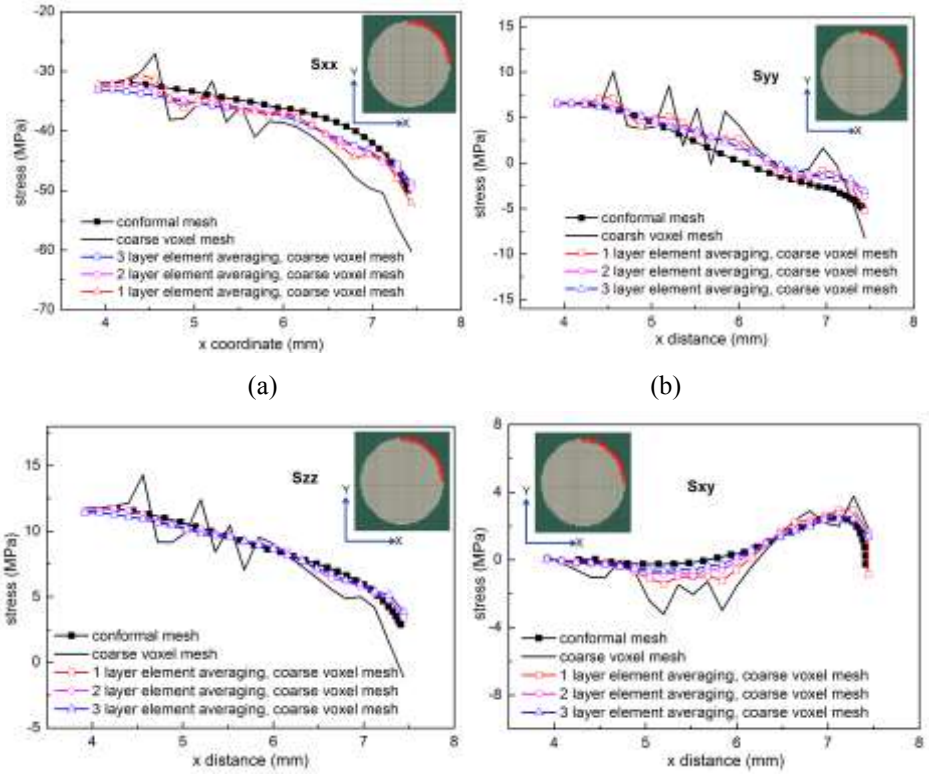

Fig. 10 Effect of different averaging domains on the averaging stress along path 1 of RVE, (a) Sxx, (b) Syy, (c) Szz, (d) Sxy

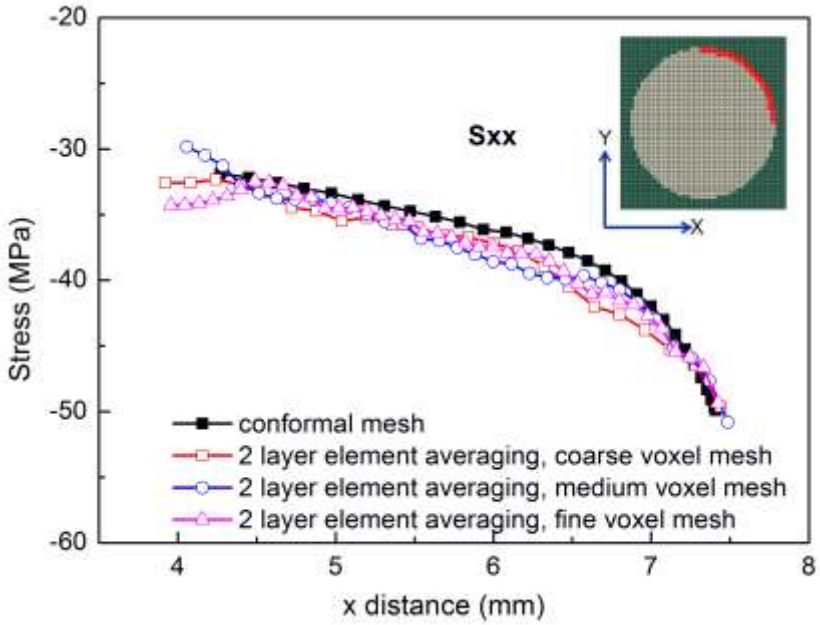

Fig. 11 Effect of mesh density on the averaging stress along path 1.

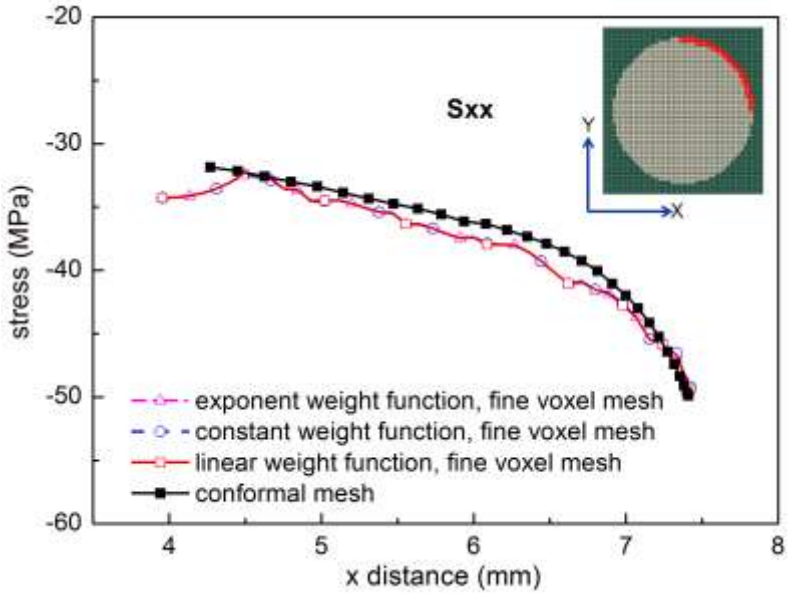

Fig. 12 Effect of weight function form on the averaging stress along path 1.

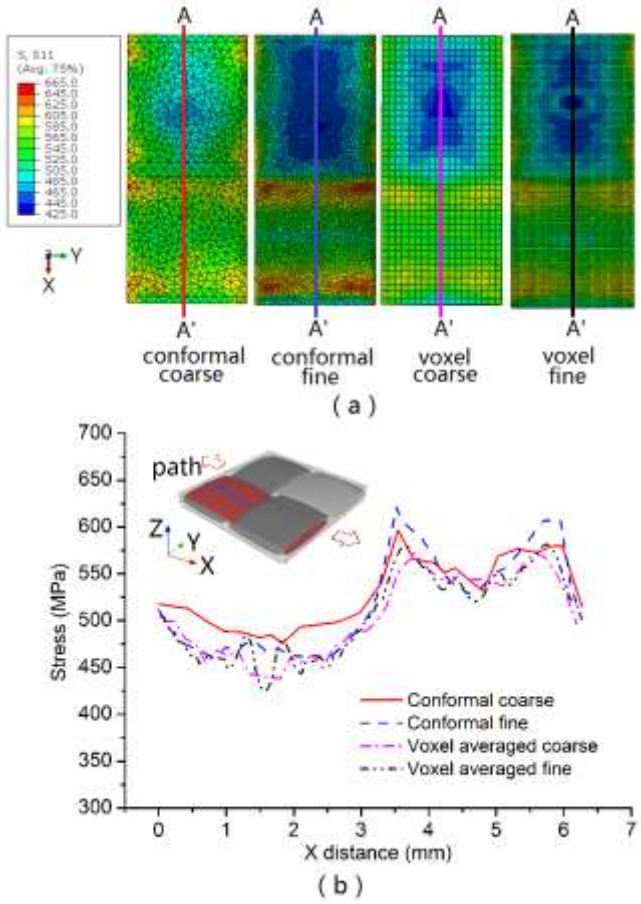

Fig. 13 Plain weave unit cell *Sxx* stress distribution on the surface of one yarn for different meshes, (a) stress contours (after stress averaging for voxel meshes), (b) stress along path A-A'.

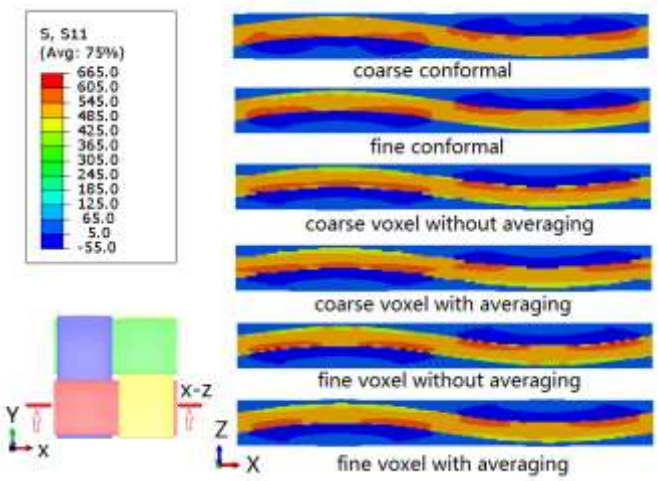

Fig. 14 S*xx* stress distribution of x-z cross-section of the plain weave textile composites.

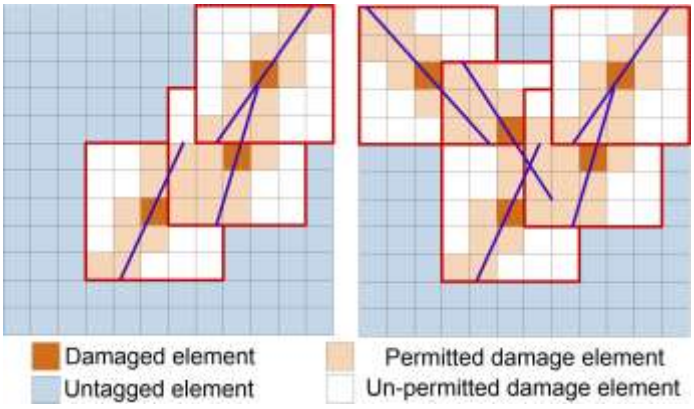

Fig. 15 Tagging damage path at the end each increment

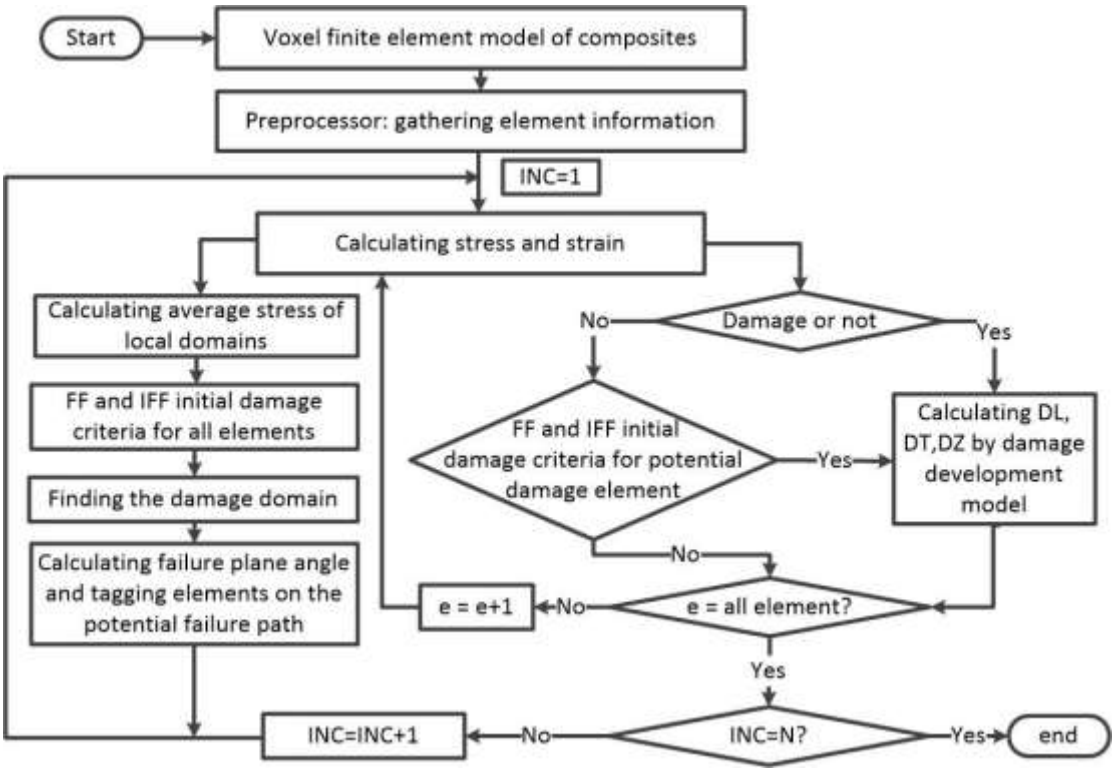

Fig. 16 Computation flow chart

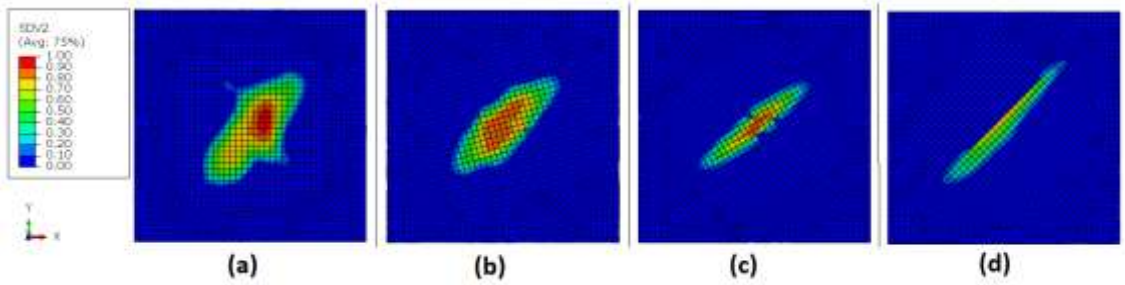

Fig. 17 The mesh Damage development path of RVE with different conformal mesh after tracking damage development path, (a)0°, (b) 15°,(c) 30°,(d)45°.

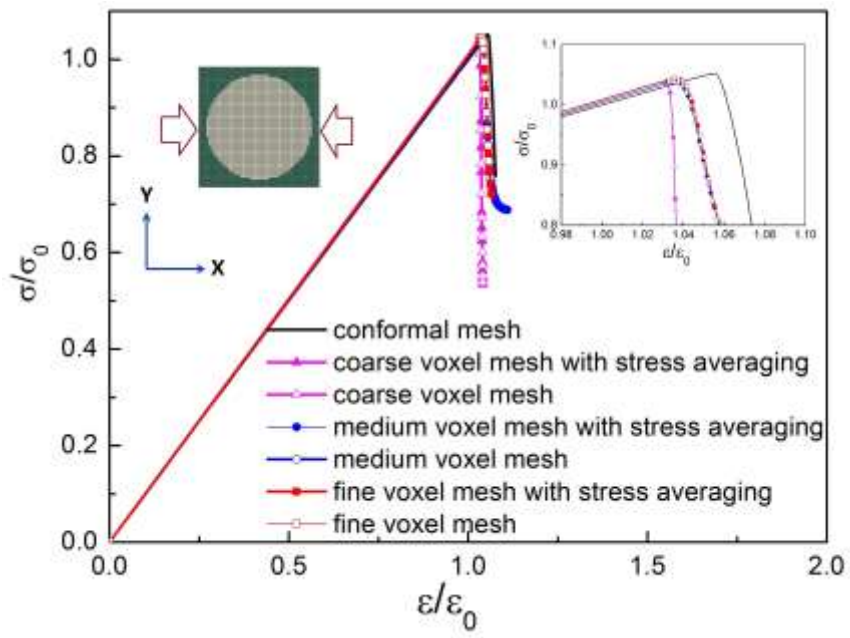

（a）

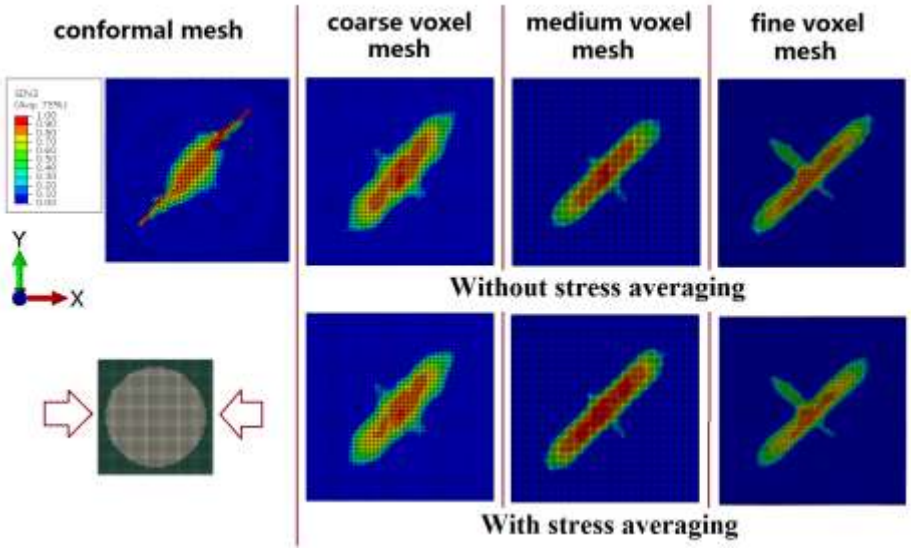

(b)

Fig. 18 Uniaxial compressive load, (a) macroscopic normalized stress and strain curve of RVE, (b) Damage and failure mode.

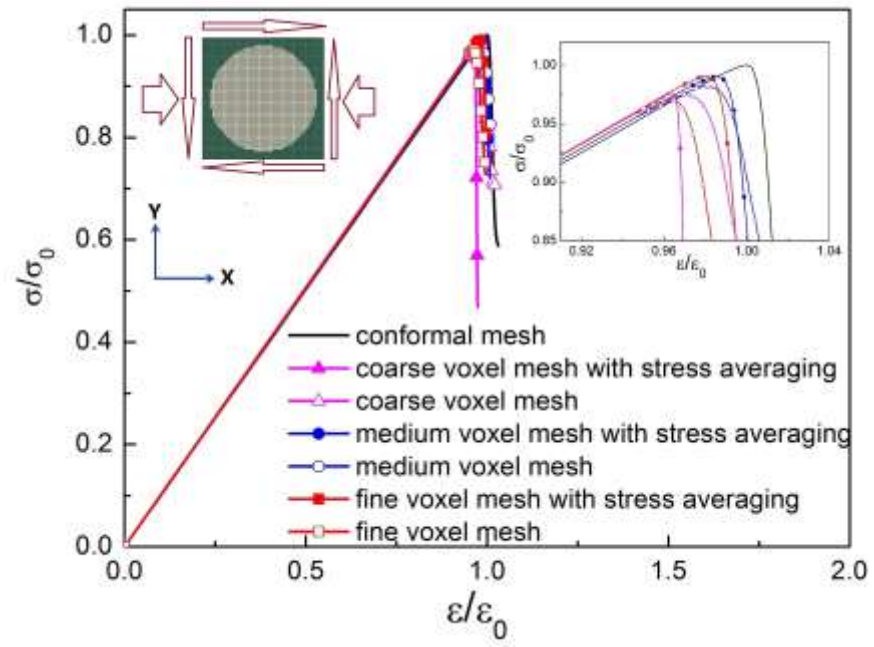

(a)

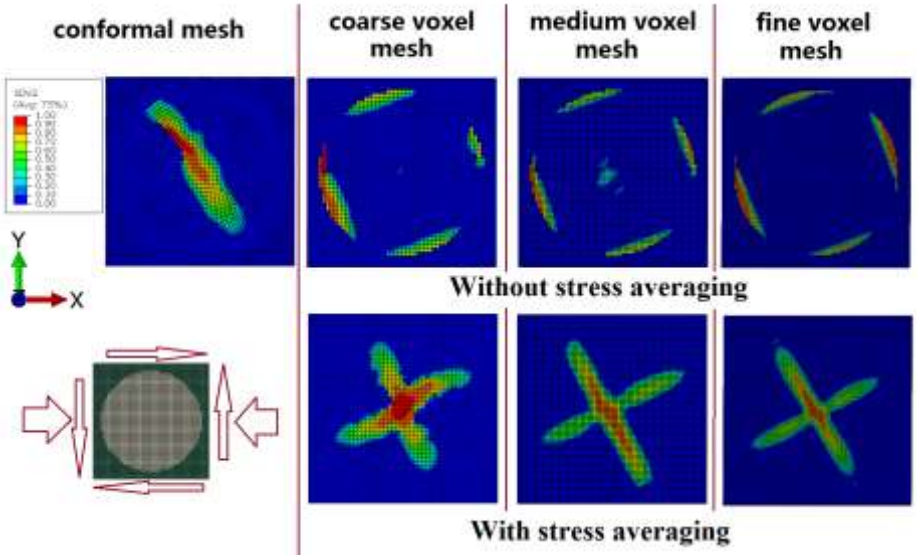

(b)

Fig. 19 Combined compressive and shear loads, (a) macroscopic normalized stress and strain curve of RVE, (b) Damage and failure mode.

Tab. 1 Maximum and minimum stresses for the three voxel mesh and one conformal mesh models with 0.5% compressive strain applied in the *x* direction.

	Conformal mesh	Voxel mesh					
		Coarse		Medium		Fine	
		Direct	Avg.	Direct	Avg.	Direct	Avg.
Sxx(Max) /MPa	-8.87	-8.90	-9.99	-7.84	-9.45	-9.17	-10.01
Sxx(Min) /MPa	-51.66	-60.15	-52.23	-61.40	-53.26	-59.85	-50.89
Syy(Max) /MPa	8.15	10.04	8.17	10.38	8.74	9.89	7.87
Syy(Min) /MPa	-20.83	-20.74	-19.28	-21.69	-19.64	-20.28	-19.54
Szz(Max) /MPa	11.82	14.30	11.65	15.10	12.65	14.36	11.70
Szz(Min) /MPa	-24.53	-24.72	-24.37	-25.42	-24.82	-24.29	-23.84
Sxy /MPa	5.50	4.57	3.91	4.87	4.35	5.25	4.73